synax: A Differentiable and GPU-accelerated Synchrotron Simulation Package

Kangning Diao,[*]
UC Berkeley, Berkeley 94720, U.S.
Tsinghua University, Beijing 100084, China

Zack Li
UC Berkeley, Berkeley 94720, U.S.

Richard D.P. Grumitt
Tsinghua University, Beijing 100084, China

Yi Mao
Tsinghua University, Beijing 100084, China

Abstract

We introduce `synax`[2], a novel library for automatically differentiable simulations of Galactic synchrotron emission. `synax` uses JAX's automatic differentiation (AD) mechanism, enabling precise computation of derivatives with respect to any model parameters. This feature facilitates powerful inference algorithms, such as Hamiltonian Monte Carlo (HMC) and gradient-based optimization, which enables inference over models that would otherwise be computationally prohibitive. Notably, we show that GPU acceleration brings a twenty-fold enhancement in efficiency, while HMC achieves a two-fold improvement over standard random walk Metropolis-Hastings when performing inference over a four-parameter test model.

1 Introduction

Galactic synchrotron emission dominates the low-frequency radio sky, spanning frequencies from MHz to GHz, and obscures cosmological signals, including those from the cosmic microwave background (CMB) [1–3], 21 cm line [4], and other line intensity measurements [e.g. 5, 6]. This emission originates from the interaction between cosmic-ray (CR) electrons and the Galactic magnetic field (GMF), with polarization altered due to Faraday rotation in the presence of the GMF and thermal electrons [7]. Consequently, while modeling synchrotron emission is essential for extracting cosmological signals, the emission itself serves as a probe for the structure of the Galactic interstellar medium (ISM) and CR transport processes [e.g. 8].

However, current synchrotron simulations, for example `hammurabi`[9, 10] and `ULSA`[11], remain computationally demanding, as they require integration along numerous sightlines with fine resolution. Recently, `JAX`[12] has emerged as a multi-platform computation framework, supporting CPUs, GPUs, TPUs, and offering automatic differentiation (AD). GPUs, designed for parallel computation, are particularly well-suited for synchrotron simulations. Moreover, AD provides access to gradients, enabling more powerful sampling and optimization algorithms, which are crucial for conducting inference on more complex models.

2 Methods

In this section, we describe the physical processes [7] and numerical techniques used to compute the synchrotron emission maps.

[*]Corresponding author.

[2]`https://synax.readthedocs.io`

Machine Learning and the Physical Sciences Workshop, NeurIPS 2024.

Synchrotron Intensity Galactic synchrotron emission is caused by the spiralling of relativistic charges in the GMF, and the cosmic-ray electron spectrum is typically modeled as a power law with a spectral index α.

Given the physical processes and assumptions, the specific intensity of synchrotron emission $I(\nu, \hat{\mathbf{n}})$ at a given frequency ν and line-of-sight (LOS) direction $\hat{\mathbf{n}}$ can be calculated with the equation

$$I(\nu, \hat{\mathbf{n}}) = \int_0^\infty j_{\rm I}(\nu, r\hat{\mathbf{n}} + \mathbf{r}_{\rm obs})dr \tag{1}$$

where r is the distance to the observer on Earth, $\mathbf{r}_{\rm obs} = (-8.3, 0.0, 0.006)$ kpc is the distance vector from the Galactic center to the Earth, and $j_{\rm I}$ is the emissivity of the synchrotron specific intensity

$$\begin{aligned} j_{\rm I}(\nu, \mathbf{r}) = &\frac{\sqrt{3}e^3 B_{\rm trans}(\mathbf{r}) N_0(\mathbf{r})}{8\pi m_e c^2} \left(\frac{4\pi\nu m_e c}{3q_e B_{\rm trans}(\mathbf{r})}\right)^{(1-\alpha)/2} \\ &\times \frac{2^{(\alpha+1)/2}}{\alpha+1}\Gamma\left(\frac{\alpha}{4} - \frac{1}{12}\right)\Gamma\left(\frac{\alpha}{4} + \frac{19}{12}\right). \end{aligned} \tag{2}$$

The amplitude of the galactic magnetic field (GMF) transverse to the LOS direction is given by $B_{\rm trans}$, q_e is the electron charge, m_e is the electron mass and c is the speed of light. We assume the number density of high-energy cosmic ray (CR) electrons, between Lorentz factors γ and $\gamma + d\gamma$, follow a power law $N(\gamma, \mathbf{r})d\gamma = N_0(\mathbf{r})\gamma^{-\alpha}d\gamma$, where $N_0(\mathbf{r})$ is the normalizing factor.

Synchrotron Polarization For the synchrotron polarization we focus on the specific intensity of polarization P. We further define the quantities Q and U, which describe the specific linear polarization, through $P = Q + iU$. We have that P is given by

$$P(\nu, \hat{\mathbf{n}}) = \int_0^\infty j_{\rm P}(\nu, r\hat{\mathbf{n}} + \mathbf{r}_{\rm obs}) e^{-2i\chi(r\hat{\mathbf{n}} + \mathbf{r}_{\rm obs})} dr, \tag{3}$$

where, $j_{\rm P}$ is the synchrotron polarized emissivity

$$\begin{aligned} j_{\rm P}(\nu, \mathbf{r}) = &\frac{\sqrt{3}e^3 B_{\rm trans}(\mathbf{r}) N_0(\mathbf{r})}{8\pi m_e c^2} \left(\frac{4\pi\nu m_e c}{3eB_{\rm trans}(\mathbf{r})}\right)^{(1-\alpha)/2} \\ &\times 2^{(\alpha-3)/2}\Gamma\left(\frac{\alpha}{4} - \frac{1}{12}\right)\Gamma\left(\frac{\alpha}{4} + \frac{7}{12}\right). \end{aligned} \tag{4}$$

$\chi(\mathbf{r})$ is the observed polarization angle of the polarized emission emitted at $\mathbf{r}$. χ can be modeled as $\chi(\mathbf{r}) = {\rm RM}\lambda^2 + \chi_0(\mathbf{r})$, where the λ is the wavelength and the rotation measure (RM) quantifies the linear rate of change of the angle χ. RM can be calculated via

$${\rm RM} = \frac{q_e^3}{2\pi m_e^2 c^4} \int_0^r n_e(r\hat{\mathbf{n}} + \mathbf{r}_{\rm obs}) B_{\rm LOS}(r\hat{\mathbf{n}} + \mathbf{r}_{\rm obs}) dr, \tag{5}$$

where n_e is the electron density and $B_{\rm LOS} = \|\mathbf{B}\cdot\hat{\mathbf{n}}\|$ is the amplitude of line-of-sight (LOS) component of the magnetic field.

The intrinsic polarization angle χ_0 is defined in [e.g. 10] as

$$\tan(\chi_0) = \frac{B_z\cos(b) - B_x\cos(l)\sin(b) - B_y\sin(l)\sin(b)}{B_y\sin(l) - B_x\cos(l)}, \tag{6}$$

where we have $\mathbf{B} = (B_x, B_y, B_z)$, l is the Galactic longitude and b is the Galactic latitude.

Integration The input fields required when simulating synchrotron emission with `synax` are: **1**. 3D Galactic magnetic field $\mathbf{B}(\mathbf{r})$, **2**. 3D thermal electron density distribution $n_e(\mathbf{r})$, **3**. Normalizing factor of CR electron distribution $N_0(\mathbf{r})$, **4**. Power-law index of the CR energy spectrum α. Unless mentioned otherwise, the power-law index α is set to be 3[13] throughout this paper.

We begin by generating the coordinates for all integration points. For the i-th sightline in the `healpix` map, the coordinates l_i, b_i are obtained using `healpy`. The intersection point between the sightline and the boundary of the 3D box is then calculated. The entire line of sight from the observer to the boundary is divided into $N_{\rm int}$ segments, and the midpoint coordinates $\{\mathbf{r}_{i,n}, n = 1, 2, \ldots, N_{\rm int}\}$ are computed for each segment. The field values $\{\mathbf{B}(\mathbf{r}_{i,n}), n_e(\mathbf{r}_{i,n}), N_0(\mathbf{r}_{i,n})\}$ are then evaluated at each of the midpoints. If an analytical function is provided for a field, its value at $\mathbf{r}_{i,n}$ is computed directly. Otherwise, we determine the field values using 3D linear interpolation, implemented with `Interpax`[3]. With these field values, χ, $j_{\rm I}$, and $j_{\rm P}$ can be computed at each $\mathbf{r}_{i,n}$ using equations 2-6.

[3] `https://interpax.readthedocs.io/en/latest/`

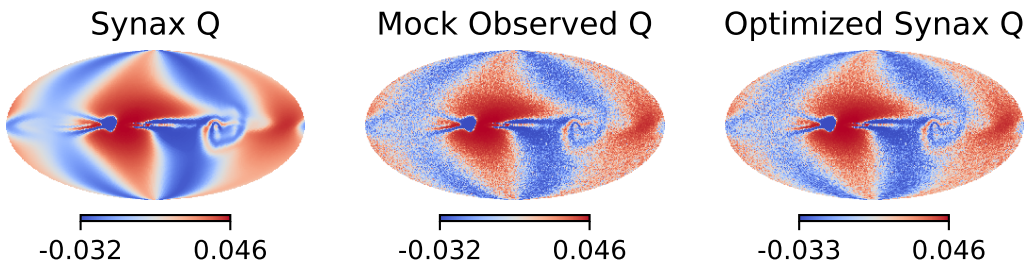

Figure 1: From right to left: simulated synchrotron Q map with WMAP **B**, mock observation, and optimized synchrotron Q map, N_0 models and YMW16 n_e model at 2.4 GHz. The map has NSIDE = 64 and $N_{\rm int} = 512$ with the units of K.

Summing along the sightline and multiplying by the segment length Δr_i yields the specific intensity maps I, Q, and U.

3 Accelerated Inference with `synax`

In this section we demonstrate the performance of `synax` when performing inference using gradient-based algorithms on two test cases. In the first example, we use the No-U-Turn sampler [NUTS, 14], a variant of gradient-based sampling method, Hamiltonian Monte Carlo [HMC, see e.g. 15], to obtain the posterior distributions for model parameters. The sampler is implemented in `Blackjax`[16][4]. In the second example we move beyond sampling parameters of analytical models, and consider using gradient-based optimization on extremely high-dimensional 3D grids.

Model Setup In our mock observation, we simulate the $\{Q, U\}$ maps with `synax`. The N_0 model here is the one adopted by Wilkinson Microwave Anisotropy Probe (WMAP) [17, 18], $N_0(\mathbf{r}) = C_0 e^{-\rho/h_r} \mathrm{sech}^2(z/h_z)$. We fix the free parameter $\{h_r, h_z\} = \{5, 1\}$ kpc, as the original WMAP parameter values. The C_0 is fixed by $N_{0,\rm Earth} = 4.0 \times 10^{-5} \mathrm{cm}^{-3}$ [e.g. 19]. The n_e model is the YMW16 model [20]. The **B** model is also the WMAP model [18],

$$\mathbf{B}(\rho, \phi, z) = b_0[\cos(\psi(\rho))\cos(\chi_B(z))\hat{\rho} + \sin(\psi(\rho))\cos(\chi_B(z))\hat{\phi} + \sin(\chi_B(z))\hat{z}].$$

The free parameters in the model are fixed as $\{b_0, \psi_0, \psi_1, \chi_{B,0}\} = \{1.2 \text{ gauss}, 0.4712 \text{ rad}, 0.0157 \text{ rad}, 0.4363 \text{ rad}\}$. We simulate the maps with NSIDE = 64 and $N_{\rm int} = 512$, corresponding to a resolution from 0.010 to 0.056 kpc. The simulated Q map is shown in the right panel of Figure 1. A mock observation is then created by adding Gaussian noise with noise standard deviation $\sigma_n = 1$ mK, as is shown in the middle panel of Figure 1.

We then use `synax` to infer **B**. The n_e and N_0 inputs are identical to the simulation, while we keep $N_{\rm int} = 512$ to avoid the numerical error from insufficient resolution. We set the prior for these parameters as $b_0 \sim \mathcal{U}[0, 10], \psi_0 \sim \mathcal{U}[0, \pi/2], \psi_1 \sim \mathcal{U}[0, \pi/2], \chi_{B,0} \sim \mathcal{U}[0, \pi/2]$, where $\mathcal{U}[a, b]$ represents a flat prior from a to b. The noise in the simulated observations is Gaussian and independent between pixels. The likelihood for this model is therefore the Gaussian likelihood with standard deviation $\sigma = 1$ mK for each pixel. Therefore, the log-likelihood $\log \mathcal{L}$ is

$$\log \mathcal{L} = \sum_i \left(\frac{(Q_i - Q_{i,\rm obs})^2}{2\sigma^2} + \frac{(U_i - U_{i,\rm obs})^2}{2\sigma^2} \right) + C \tag{7}$$

where C is a normalization constant.

Sampling with NUTS We first sample the posterior of the WMAP analytical **B** field model parameters, namely $\{b_0, \psi_0, \psi_1, \chi_{B,0}\}$, with NUTS on a GPU. We run NUTS for 600 iterations and leave the first 100 as burn-in. Posterior summary statistics are shown in Table 1. The Gelman-Rubin $\hat{r}$ [21] for the samples are all below 1.01, and the effective sample size (ESS) is of the same order of sampling iterations. We can therefore be confident that we have converged on the stationary distribution, and the corresponding posterior samples are generated with minimal auto-correlation. We find the accuracy,

[4] `https://blackjax-devs.github.io/blackjax/index.html`

Parameter	Best-fit	Accuracy	$\hat{r}$	ESS
b_0	1.2002 ± 0.0003	0.01%	1.003	553.35
ψ_0	0.4707 ± 0.0004	-0.11%	1.003	503.94
ψ_1	0.0147 ± 0.0012	-6.48%	0.999	310.59
$\chi_{0,B}$	0.4367 ± 0.0014	0.09%	1.006	252.37

Table 1: Posterior summary statistics obtained with NUTS.

Method	b_0	ψ_0	ψ_1	$\chi_{0,B}$
NUTS GPU	1.90	1.73	1.07	0.87
NUTS CPU	0.09	0.06	0.04	0.03
RWMH GPU	9.49	13.30	7.34	0.37
RWMH CPU	0.14	0.20	0.11	0.01

Table 2: ESS per second for NUTS and RWMH after burn-in.

defined by $(\bar{p} - p_{\text{true}})/p_{\text{true}}$, is very close to 0 as is listed in Table 1, except ψ_1 because of its small magnitude. The true parameter mostly lies in the 1σ confidence level of the posterior.

We also ran NUTS on CPU and simple Random Walk Metropolis-Hastings (RWMH) on GPU and CPU to provide a benchmark. The ESS per second for each parameter is shown in Table 2. On CPU, a single `synax` realization with 128 threads took $\sim$ 200 ms to finish. Typically, to ensure convergence, the ESS for all parameters must be beyond a certain threshold. Comparing the minimum ESS per second (i.e. ESS per second for $\chi_{0,B}$), we obtain approximately a 20× speed-up with the GPU acceleration, and NUTS brings 2× extra improvement in this simple test model. The improvements from using gradient-based sampling methods such as NUTS will be more apparent for higher dimensional sampling problems [22, 23].

Optimizing 3D Grids The WMAP analytical modeling of the GMF [18] focuses on the large scale structure of the Galaxy, but does not account for small scale features e.g., turbulence in the Galactic plane. In this study, we consider a more general approach by directly optimizing the 3D **B** grids based on mock observations. The grid consists of $128 \times 128 \times 32$ voxels, with a corresponding box size of $(40, 40, 10)$ kpc. Our goal is to optimize the 3D grids to maximize the log-likelihood $\log \mathcal{L}$. Due to the high dimensionality ($\sim 5 \times 10^6$) of this problem, we employ the ADAM optimizer [24] implemented via `Optax`[12][5]. To prevent overfitting, optimization is halted after 200 iterations. The optimized synchrotron map is presented in the right panel of Figure 1. Due to the high flexibility of the grid representation, noise features are also reproduced, indicating significant overfitting. The

[5] `https://optax.readthedocs.io/en/latest/`

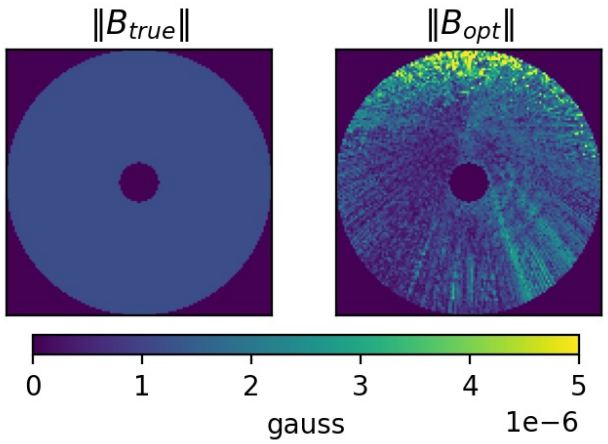

Figure 2: Left: true **B** field magnitude at z = 0 kpc. Right: optimised **B** field magnitude at z = 0 kpc.

optimized **B** magnitude is shown in Figure 2, where it is evident that the **B** field fluctuates considerably to replicate the noise features.

Testing with a 16-parameter Model To assess the performance of `synax` with gradient-based sampling methods in higher dimensions, we construct a mock observation using a 16-parameter model. This model is generated by stacking four WMAP magnetic field models, each with different parameters. We compare the performance of the NUTS and RWMH algorithms on GPU for sampling this more complex model. NUTS achieves a minimum ESS per second of 1.53×10^{-2}, whereas RWMH fails to converge within 12 hours, demonstrating a clear advantage of NUTS for efficiently exploring high-dimensional parameter spaces.

4 Conclusion

In this paper, we introduce `synax`, a novel synchrotron intensity and polarization simulation package that, for the first time, leverages automatic differentiation (AD) and hardware acceleration. GPU acceleration significantly enhances computational speed, while AD enables efficient sampling algorithms for Bayesian posterior inference. The incorporation of 3D grids as a representation of fields within AD-based optimization algorithms allows for the characterization of more complex magnetic field structures.

While this work incorporates the radiative transfer equation, secondary effects such as scattering [e.g. 25, 26] have been omitted and will be addressed in future updates. Additionally, while free-free emission and absorption—negligible beyond the GHz range—are not considered here, they play a critical role in low-frequency observations. Future iterations of `synax` will include these processes to extend its applicability to the low-frequency domain.

Acknowledgments and Disclosure of Funding

KND, RDPG and YM are supported by the National SKA Program of China (grant No. 2020SKA0110401) and NSFC (grant No. 11821303). This work is also supported by U.S. Department of Energy, Office of Science, Office of Advanced Scientific Computing Research under Contract No. DE-AC02-05CH11231 at Lawrence Berkeley National Laboratory to enable research for Data-intensive Machine Learning and Analysis.

A Accuracy and Efficiency Comparison with `hammurabi`

We validate our model on a simple scenario [10] at $\nu = 2.4$ GHz. In this model, the fields are homogeneous, $\mathbf{B}(\mathbf{r}) = (6 \times 10^{-6}\text{gauss}, 0, 0)$, $n_e(\mathbf{r}) = 0.01\,\text{cm}^{-3}$, and $N_0(\mathbf{r}) = 4.01 \times 10^{-5}\text{cm}^{-3}$ within a spherical region of the radius $R_0 = 4$ kpc of the Earth, and zero outside. (Note that these fields are not spherically symmetric with respect to the Galactic center.) In this case, the emission intensity before Faraday rotation $\{I, Q_0, U_0\}$ becomes:

$$\begin{aligned} I &= j_\text{I} R_0, \\ Q_0 &= j_\text{P} R_0 \cos(2\chi_0), \\ U_0 &= j_\text{P} R_0 \sin(2\chi_0), \end{aligned} \tag{8}$$

since $j_\text{I}, j_\text{P}, \chi_0$ are constants along a sightline. The Q_0 and U_0 will be altered by

$$Q + iU = (Q_0 + iU_0) \int_0^{R_0} \frac{1}{R_0} e^{2i\lambda^2 r' n_e B_\text{LOS} q_e^3 / 2\pi m_e^2 c^4}\, dr' \tag{9}$$

Thus, $\{I, Q, U\}$ maps can be calculated analytically.

We then simulate the $\{I, Q, U\}$ maps with `synax`, and for this demonstration we specify NSIDE = 64 and $N_\text{int} = 1024$. The length of the box is $(40, 40, 10)$ kpc. We set the input as analytical functions and the results are shown in Figure 3. The typical scale of absolute residuals is below 1% of the signal scale, and the relative error, defined by $\epsilon_\text{rel} = 2(X_\text{sim} - X_\text{ana})/(X_\text{sim} + X_\text{ana})$ where X_sim is the simulated map and X_ana is the analytical map, is also mostly at the percentage level, except for sightlines with field value very close to zero. We note that the residuals are all below 1 mK, suggesting that `synax` with function input has no significant bias with mK noise level observations.

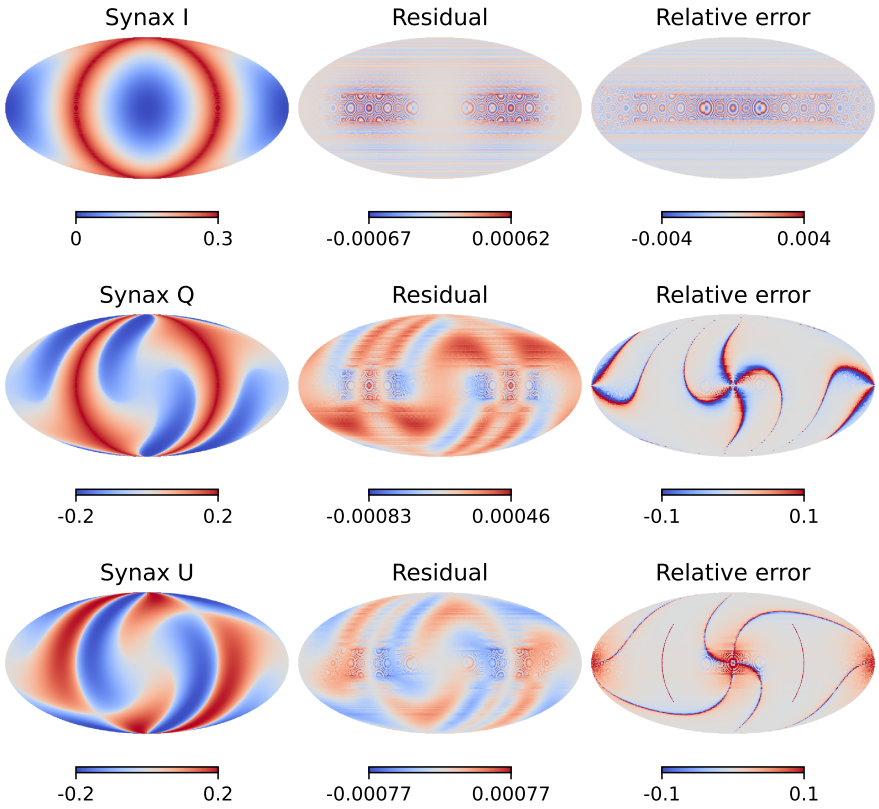

Figure 3: Accuracy test with homogeneous $\{\mathbf{B}(\mathbf{r}), n_e(\mathbf{r}), N_0(\mathbf{r})\}$ fields with callable field generators. The left panel shows the synchrotron $\{I, Q, U\}$ maps generated by `synax`, the middle panel shows the residual between `synax` and theoretical value, and the right panel shows the relative error between `synax` and the theoretical value. All `healpix` maps are in units of Kelvin.

Our code is based on `JAX` [12] and can run on multiple platforms including CPU, GPU, and TPU. `synax` uses $\sim$ 300 ms to generate the emission map on an NVidia Tesla A100 after just-in-time (JIT) compilation. For comparison, it takes $\sim 30,000$ ms for the MPI-parallelized CPU-based code `hampyx` [10] to run with 64 threads on an AMD `milan` CPU, while it only integrates with 100 points along each sightline. `synax` obtains the same level of accuracy as `hammurabi`, with the standard deviation of residuals for the $\{I, Q, U\}$ maps with `synax` being $\{1.6\times10^{-4}, 2.0\times10^{-4}, 2.0\times10^{-4}\}$, while with `hammurabi` the standard deviation of residuals is $\{1.6\times10^{-5}, 5.6\times10^{-4}, 6.0\times10^{-4}\}$, respectively. `synax` gains $\gtrsim$ 100 times improvement in wall clock time, along with access to the gradient with AD.

References

[1] N. Krachmalnicoff, E. Carretti, C. Baccigalupi, G. Bernardi, S. Brown, B.M. Gaensler et al., *S-PASS view of polarized Galactic synchrotron at 2.3 GHz as a contaminant to CMB observations*, *A&A* **618** (2018) A166 [1802.01145].

[2] M.E. Jones, A.C. Taylor, M. Aich, C.J. Copley, H.C. Chiang, R.J. Davis et al., *The C-Band All-Sky Survey (C-BASS): design and capabilities*, *MNRAS* **480** (2018) 3224 [1805.04490].

[3] J.A. Rubiño-Martín, F. Guidi, R.T. Génova-Santos, S.E. Harper, D. Herranz, R.J. Hoyland et al., *QUIJOTE scientific results - IV. A northern sky survey in intensity and polarization at 10-20 GHz with the multifrequency instrument*, *MNRAS* **519** (2023) 3383 [2301.05113].

[4] A. Liu and J.R. Shaw, *Data Analysis for Precision 21 cm Cosmology*, *PASP* **132** (2020) 062001 [1907.08211].

[5] Y. Gong, M. Silva, A. Cooray and M.G. Santos, *Foreground Contamination in Lyα Intensity Mapping during the Epoch of Reionization*, *ApJ* **785** (2014) 72 [1312.2035].

[6] A.S. Maniyar, A. Gkogkou, W.R. Coulton, Z. Li, G. Lagache and A.R. Pullen, *Extragalactic CO emission lines in the CMB experiments: A forgotten signal and a foreground*, *Phys. Rev. D* **107** (2023) 123504 [2301.10764].

[7] G.B. Rybicki and A.P. Lightman, *Radiative Processes in Astrophysics*, New York: Wiley (1986).

[8] M. Unger and G.R. Farrar, *The Coherent Magnetic Field of the Milky Way*, *ApJ* **970** (2024) 95 [2311.12120].

[9] A. Waelkens, T. Jaffe, M. Reinecke, F.S. Kitaura and T.A. Enßlin, *Simulating polarized Galactic synchrotron emission at all frequencies. The Hammurabi code*, *A&A* **495** (2009) 697 [0807.2262].

[10] J. Wang, T.R. Jaffe, T.A. Enßlin, P. Ullio, S. Ghosh and L. Santos, *hammurabi X: Simulating Galactic Synchrotron Emission with Random Magnetic Fields*, *ApJS* **247** (2020) 18 [1907.00207].

[11] Y. Cong, B. Yue, Y. Xu, Q. Huang, S. Zuo and X. Chen, *An Ultralong-wavelength Sky Model with Absorption Effect*, *ApJ* **914** (2021) 128 [2104.03170].

[12] DeepMind, I. Babuschkin, K. Baumli, A. Bell, S. Bhupatiraju, J. Bruce et al., *The DeepMind JAX Ecosystem*, 2020.

[13] C.L. Bennett, R.S. Hill, G. Hinshaw, M.R. Nolta, N. Odegard, L. Page et al., *First-Year Wilkinson Microwave Anisotropy Probe (WMAP) Observations: Foreground Emission*, *ApJS* **148** (2003) 97 [astro-ph/0302208].

[14] M.D. Hoffman and A. Gelman, *The No-U-Turn Sampler: Adaptively Setting Path Lengths in Hamiltonian Monte Carlo*, *arXiv e-prints* (2011) arXiv:1111.4246 [1111.4246].

[15] M. Betancourt, *A Conceptual Introduction to Hamiltonian Monte Carlo*, *arXiv e-prints* (2017) arXiv:1701.02434 [1701.02434].

[16] A. Cabezas, A. Corenflos, J. Lao and R. Louf, *Blackjax: Composable Bayesian inference in JAX*, 2024.

[17] R. Drimmel and D.N. Spergel, *Three-dimensional Structure of the Milky Way Disk: The Distribution of Stars and Dust beyond 0.35 R_{solar}*, *ApJ* **556** (2001) 181 [astro-ph/0101259].

[18] L. Page, G. Hinshaw, E. Komatsu, M.R. Nolta, D.N. Spergel, C.L. Bennett et al., *Three-Year Wilkinson Microwave Anisotropy Probe (WMAP) Observations: Polarization Analysis*, *ApJS* **170** (2007) 335 [astro-ph/0603450].

[19] A.W. Strong, I.V. Moskalenko and V.S. Ptuskin, *Cosmic-Ray Propagation and Interactions in the Galaxy*, *Annual Review of Nuclear and Particle Science* **57** (2007) 285 [astro-ph/0701517].

[20] J.M. Yao, R.N. Manchester and N. Wang, *A New Electron-density Model for Estimation of Pulsar and FRB Distances*, *ApJ* **835** (2017) 29 [1610.09448].

[21] A. Gelman and D.B. Rubin, *Inference from Iterative Simulation Using Multiple Sequences*, *Statistical Science* **7** (1992) 457.

[22] A. Gelman, W.R. Gilks and G.O. Roberts, *Weak convergence and optimal scaling of random walk metropolis algorithms*, *The annals of applied probability* **7** (1997) 110.

[23] A. Beskos, N.S. Pillai, G.O. Roberts, J.M. Sanz-Serna and A.M. Stuart, *Optimal tuning of the Hybrid Monte-Carlo Algorithm*, *arXiv e-prints* (2010) arXiv:1001.4460 [1001.4460].

[24] D.P. Kingma and J. Ba, *Adam: A Method for Stochastic Optimization*, *arXiv e-prints* (2014) arXiv:1412.6980 [1412.6980].

[25] T.W. Jones and S.L. O'Dell, *Transfer of polarized radiation in self-absorbed synchrotron sources. I. Results for a homogeneous source.*, *ApJ* **214** (1977) 522.

[26] J.Y.H. Chan, K. Wu, A.Y.L. On, D.J. Barnes, J.D. McEwen and T.D. Kitching, *Covariant polarized radiative transfer on cosmological scales for investigating large-scale magnetic field structures*, *MNRAS* **484** (2019) 1427 [1901.04581].